This is a preprint, the final version is subject to change, of the American Mineralogist (MSA)
Cite as Authors (Year) Title. American Mineralogist, in press.
DOI: http://dx.doi.org/10.2138/am-2018-6141

Laboratory and field characterization of visible to near infrared spectral reflectance of nitrate minerals from the Atacama Desert, Chile and implications for Mars

Fan Wang[1, 2], Brenda B. Bowen[3*], Ji-Hye Seo[4], Greg Michalski[2, 4]

[1]School of Environment and Energy, Peking University Shenzhen Graduate School, Shenzhen, Guangdong 518055, China

[2]Department of Earth, Atmospheric and Planetary Sciences, Purdue University, West Lafayette, Indiana 47907, USA

[3]Department of Geology and Geophysics, University of Utah, Salt Lake City, Utah 84112, USA

[4]Department of Chemistry, Purdue University, West Lafayette, Indiana 47907, USA

[*]Corresponding author. E-mail: **brenda.bowen@utah.edu**

ABSTRACT

Large amounts of nitrate salts occur in very specific environments and somewhat rare hyper-arid conditions, which may provide clues to fundamentally different nitrogen cycling and life survival mechanisms. Remote detection of ancient and modern nitrates on Earth and on other planetary bodies where they may occur requires a detailed understanding of their visible to near infrared (VNIR) spectral signatures. This study explores the VNIR spectral characteristics of several synthetic nitrate salts, sulfate minerals and nitrate-bearing field samples from the Atacama Desert, Chile to identify diagnostic spectral features of nitrate and possible interferences from other co-existing minerals. Results indicated that most of the nitrate salts have characteristic absorptions around 1.81, 1.94, 2.06, 2.21 and 2.42 μm, and a significant positive correlation exists between the continuum-removed band depths of the 2.42 μm absorption and nitrate

contents for the Atacama regolith samples, especially for samples with >10 wt% nitrate. The five absorption features of nitrate in the field spectra collected from multiple nitrate-rich regions in the Atacama Desert were then evaluated to determine the variabilities in these features in natural settings, while the band depth of 2.42 μm absorption was further calculated on the continuum-removed field spectra to estimate the nitrate abundances at the study sites. However, the VNIR spectral absorptions of nitrate tend to overlap with those of hydrated sulfate or oxychlorine salts, making the spectral identification of sulfate, oxychlorine or nitrate ambiguous. This work will supplement spectral libraries where nitrate spectra are lacking, and have implications for future comparisons to planetary spectra to search for potentially life-related nitrate on Mars.

Keywords: nitrate; Atacama Desert; Mars; visible to near infrared reflectance

This is a preprint, the final version is subject to change, of the American Mineralogist (MSA)
Cite as Authors (Year) Title. American Mineralogist, in press.
DOI: http://dx.doi.org/10.2138/am-2018-6141

INTRODUCTION

The Atacama Desert in northern Chile has been proposed as an important Mars analog due to its hyper-arid climate (Navarro-González et al., 2003). The hyper-aridity in the core of the Atacama Desert is the combined result of the rain shadow effects created by the Coastal Range and the Andes, the cold upwelling Peru Current, and the south Pacific subtropical anticyclone (Houston and Hartley, 2003; Houston, 2006). The Atacama is known to have highly saline soils containing the largest nitrate deposits in the world (Ericksen, 1981), which is unique and mainly due to that the hyper-arid climate minimizes leaching losses and preserves nitrate and other soluble salts, such as chloride, sulfate and perchlorate. While the hyper-aridity stabilizes the saline soils in the Atacama, the origins of massive soluble salts were long disputed before recent isotopic studies definitely attributed these soluble salts to atmospheric origins (Bao and Gu, 2004; Bao et al., 2004; Michalski et al., 2004; Wang et al., 2016). Oxides of nitrogen, sulfur and chlorine in the atmosphere can be oxidized via photochemical pathways (i.e. chemical reactions caused by light) into their stable end products as nitrate, sulfate and perchlorate, respectively, which can subsequently be deposited onto the ground surface (Seinfeld and Pandis, 2006). As recent development of triple oxygen isotope analysis allowed the source apportionment of soluble salts in the soil based on distinctive oxygen isotope signatures in different sources, the Atacama salts were revealed to have similar oxygen isotope compositions to their atmospheric equivalents, suggesting their predominant origin from atmospheric deposition. Indeed, in hyper-arid environments such as the Atacama, where biological and hydrological activities should be extremely low, atmospheric deposition, especially dry deposition, may be one of the main processes that

control surface geomorphology (Ewing et al., 2006). The successive detection of sulfate, chloride and perchlorate on the surface of Mars (Squyres et al., 2004; Osterloo et al., 2008; Hecht et al., 2009), similar to the existence of chloride, perchlorate and sulfate deposits in the Atacama, hints that analogous deposition processes may be occurring on Mars.

Whether there are also nitrate deposits occurring on Mars as in the Atacama is of great interests to the scientific community because nitrate is an important part of biogeochemical cycling on Earth and may be indicative of past life on Mars. A number of studies have proposed mechanisms that could lead to photochemical production of nitrate in a Martian atmosphere (Yung et al., 1977; Nair et al., 1994) and possible incorporation of nitrate into the Martian regolith (Banin et al., 1997; Mancinelli, 1996). Nevertheless, the search of nitrate on Mars had proved to be very difficult until the Sample Analysis at Mars (SAM) instrument suite on the Mars Science Laboratory (MSL) Curiosity rover recently detected NO that was believed to be released from the breakdown of nitrates during pyrolysis (Stern et al., 2015). However, other nitrogen-containing compounds could also release NO as samples are heated by SAM, which complicates interpretations of nitrate abundances in Martian soils from SAM analysis. In addition, SAM analysis is confined to a relatively small region that is limited by the activities of the Curiosity rover and the time and costs of each analysis. Instead, orbital spectral sensors can provide an important tool for investigating planetary-scale presence or absence of nitrate on Mars. However, use of these sensors requires a detailed understanding of the spectral characterization of nitrate minerals and how they vary in natural heterogeneous environments.

Spectral characterization of nitrate has previously been reported (Hovis, 1966; Ericksen and Mrose, 1970; Harris et al., 1990; Sutter et al., 2007) and there have been several trials using nitrate spectral characteristics to determine nitrate in soil or vegetation leaves (Ehsani et al., 2001; Boonmung and Riley, 2003; Jahn et al., 2006). However, these trials were primarily laboratory investigations focusing on representative spectral features in the mid-infrared region, providing limited comparisons for Martian sensors that usually measure reflectance in the visible to near infrared (VNIR) region. To our knowledge, only two works to date (Sutter et al., 2007; Cloutis et al., 2016) discussed the possibility of nitrate detection using VNIR hyperspectral remote sensing techniques on Mars. Sutter et al. (2007) systematically compared the laboratory spectra (0.35-25 μm) of several minerals commonly existing in the Atacama Desert, including nitratine ($NaNO_3$), to the remotely sensed spectra of the Martian soil to help identify mineral compositions, but they were mainly concentrated on infrared analysis of Atacama soils with very little attention to nitrate, especially less attention extended to nitrate detection on Mars. Cloutis et al. (2016) measured the reflectance spectra (0.35-20 μm) of synthetic KNO_3, $NaNO_3$ and NH_4NO_3 compounds and summarized the current and future hyperspectral imaging systems that could be adopted for the search of nitrate on Mars, but they rarely addressed how nitrate spectra are impacted by interferences from co-existing minerals. In summary, there are still lacks of VNIR spectra of a wide selection of nitrate compounds in spectral libraries, understandings on how the nitrate absorptions are interfered by co-existing minerals, or field assessments to couple laboratory investigations with remote sensing data (Moorcroft et al., 2001; Sinfield et al., 2010). Therefore, this study is designed to characterize the VNIR absorption features of nitrate, evaluate the interferences of nitrate

absorptions from co-existing minerals, and develop a scheme to detect the presence of nitrate and quantify the nitrate abundances based on reflectance spectra at the field scale, which will provide perspectives into the nitrate search via remote sensing on Mars and in other similar environments.

METHODS

Laboratory spectra collection: A number of pure synthetic nitrate salts, and sulfate minerals (potentially interfering minerals for nitrate spectral characterization) were obtained for laboratory spectral analysis. Sixteen reagent grade metal nitrate salts (Table 1) and mirabilite (Na_2SO_4•$10H_2O$) were purchased from authorized commercial retailers. Though some of the 16 metal nitrates might be rare in most terrestrial systems, they were included to supplement the database and investigate whether characteristic nitrate features or spectral shifts are prominent for a wide selection of nitrate compounds. Delicate platy darapskite crystals ($Na_3NO_3SO_4$•H_2O) were precipitated out through gradual evaporation of the mixture of saturated $NaNO_3$ and Na_2SO_4 solutions under warm ambient temperature (approximately 20°C). Darapskite and mirabilite samples were heated in a muffle furnace at 60°C for 2 hours to remove any adsorbed water before measurements in order to look at the characteristic absorption features in anhydrous forms of minerals. These salt or mineral samples were all gently ground to powders of homogenous grain sizes (<0.18 mm) for further analysis.

Atacama regolith samples were collected from two trenches in the Baquedano region, called “long trench” (LT) and “small trench” (ST), respectively, and one incised lahar paleosediment profile in the Chug-Chug geoglyphs field, called “Chug-Chug paleosediment” (CCP). The LT site (22.88°S, 69.64°W, 1500 m a.s.l.) is a 225 cm deep

trench stretching several kilometers (see more details in Wang et al. (2015)), while the ST site (22.83°S, 69.72°W, 1501 m) is a ~2 m long and 2.35 m deep trench unit. These two trench sites are located in the Baquedano basin that is characterized by flat, rugged and barren alluvial surfaces, receiving <0.4 mm precipitation annually (Houston, 2006). No erosional evidence was observed at either trench site, and all the regolith material were loosely cemented such that they could be sampled with hand shovels. The CCP site (22.04°S, 69.13°W, 2423 m) is a 4 m high profile located in an ancient riverbed with sediment channels preserved in the upper stratum and a spring nearby with sparse vegetation. All horizons of the CCP profile consisted of well-cemented rock-like sediment, requiring electric saws for sampling. The trenches and paleosediment outcrop were sampled from the bottom (2-4 m) to the surface at ~5 cm vertical resolution, totaling 43, 55 and 72 samples from the LT, ST and CCP profiles, respectively.

The powdery salts and minerals, and intact regolith samples were analyzed in the laboratory at Purdue University using an ASD FieldSpec® 3 reflectance spectrometer (Analytical Spectral Devices Inc., Boulder, Colorado) that measures reflectance from 0.35-2.5 μm. Reflectance was measured relative to a white reflectance standard Spectralon plate (Labsphere Inc., North Sutton, UK) using the instrument's fiber optic contact probe that has a 1 cm diameter spot size and 8° field of view. Lab measurements were made in a dark room using artificial illumination of white light emitted from a tungsten filament lamp (~3400°K color temperature). The wavelength scanning interval is 1.4 nm in the spectral range of 0.35-1.0 μm and 2 nm in the spectral range of 1.0-2.5 μm, while the spectral resolution ranges from 3-10 nm. 30 scan acquisitions were set to yield an average spectrum for each spectral measurement during the indoor operation to

improve the signal-to-noise ratio. Continuum was further removed of the measured reflectance spectra by dividing the reflectance values of an established convex hull into the actual reflectance spectrum (Kokaly and Clark, 1999) to isolate the absorption features. The absorption band depth was calculated by subtracting the relative reflectance value at the band minimum of each absorption feature from 1 in the continuum-removed spectrum.

In addition, one gram of each regolith sample was homogenized, ground by ball mill or hand, and vortexed to extract soluble salts with 45 mL Milli-Q Millipore^{TM} water (ultrapure>16MΩ). The anion (chloride, nitrate and sulfate) contents in the extracts were analyzed using a Dionex-500 ion chromatography with suppressed conductivity detection (Dionex Corp., Sunnyvale, CA, USA). Blank controls and external standard calibration were performed for quality control and assurance. The measurement uncertainties for each anion content were typically <5% based on replicate analysis of standards and calibrations. Correlation analysis between the absorption band depths and anion contents of samples from the three profiles (LT, ST and CCP) was performed using the statistical software package PASW Statistics 18.0 (SPSS Inc., Chicago, IL, USA).

Field spectra collection: In situ field based spectra were collected by the ASD FieldSpec® 3 reflectance spectrometer using a pistol grip with the attached fiber optic cable for one soil pit (Baquedano pit 1), three mine tailings (Baquedano mine, Sierra Gorda mine and Tama mine), and two salars (Salar de Carmen and Salar de Grande). These sites were selected to collect field spectra due to that their textural and environmental characteristics suggested possible presence of surface nitrate efflorescent salts. The measurements were taken at a distance of 5-10 cm from the samples around

174 noon on clear days, and the white reflectance standard Spectralon plate was measured
175 every 2-3 minutes to minimize the effects of changing illumination and meteorological
176 conditions. 100 scan acquisitions were set to yield an average spectrum for each field
177 spectral measurement to improve the signal-to-noise ratio. In addition, 6 returned field
178 samples from Baquedano pit 1, 4 from Baquedano mine, 8 from Sierra Gorda mine and
179 14 from Tama mine were measured for reflectance in the laboratory and their laboratory
180 spectra were compared to the field spectra to check their consistence.

181 The Baquedano pit 1 site (22.98°S, 69.84°W, 1400 m a.s.l), close to the LT and ST
182 sites (~20 km distance), is a ~2 m deep pit located in an alluvial fan that lacks surface
183 erosion features but has a ~15 cm deep gypsum layer developed below the surface in the
184 Baquedano region (Figure 1A). The weathered surface of the pit face was removed to
185 expose a fresh surface before 23 field spectra were collected.

186 The Baquedano mine site (23.11°S, 69.91 °W, 1432 m) is near a deserted nitrate mine,
187 and its surface of a reddish appearance is highly disturbed with big rocks exposed (Figure
188 1B). The Sierra Gorda nitrate mine site (23.07°S, 69.49°W, 1420 m) is located in the
189 Sierra Gorda region with a mine tailing ~10 m high and ~3000 m × 1200 m in size
190 (Figure 1C). The Tama mine site (20.52°S, 69.77°S, 999 m) is in a hilly terrain with
191 weathered broken rocks in the surroundings and a gentle hill slope (Figure 1D) and
192 visually similar to the Burns Cliff within Endurance Crater on Mars (Watters et al., 2011).
193 21, 26 and 27 field spectral measurements were conducted on the tops and along the cross
194 sections of the Baquedano, Sierra Gorda and Tama mine tailing profiles, respectively.

195 The Carmen site (23.65°S, 70.27°W, 524 m) is located on the western side of the
196 Salar de Carmen, a closed basin at the terminus of the broad, transverse, debris-filled

Baquedano valley drainage (Ericksen, 1981); nitrate minerals are known to periodically accumulate on the salar's surface (Whitehead, 1920). 53 field spectra were collected in total along two ~100 m long representative transects that are covered with soft, flat and yellowish surface (Figure 1E). The Grande site (21.22°S, 69.90°W, 800 m) is located on the southeastern rim of the Salar de Grande, a terminal basin filled with massive salt minerals, mainly halite (NaCl). 74 field spectra of the surfaces were taken along a ~100 m long transect over which the barren ground covered with 0.5-1 cm reddish to tannish pebbles abruptly transitions to a hummocky ground with a relief of 50 cm. The hummocky ground is mostly covered with biological crusts, while barren depression pits (~2-5 m in diameter) filled with white salt nodules (mainly halite) were sparsely scattered across the hummocky ground (Figure 1F).

RESULTS AND DISCUSSION

Nitrate characterization

The 16 pure nitrate salts are divided into two groups based on their hydration states and their 0.35-2.5 μm reflectance spectra are shown in Figure 2 while the positions of the absorption band minima in the 1.5-2.5 μm region are listed in Table 1. Sutter et al. (2007) reported that various N-O overtones/combinations could cause VNIR absorptions around 1.81, 1.94, 2.06, 2.21 and 2.42 μm (Table 2), while Cloutis et al. (2016) revealed that the positions of the absorption band minima might vary slightly in different minerals. The spectra of anhydrous $NaNO_3$ and KNO_3 salts in this study are similar to the spectrum of niter (KNO_3) archived in the USGS spectral library by Clark et al. (2007) (Figure 2A and Table 1) and the observations for $NaNO_3$ and KNO_3 by Sutter et al. (2007) and Cloutis et al. (2016). They all show prominent absorptions around 1.81, 1.94, 2.06, 2.21 and 2.42

μm despite the changes in the positions of band minima and some being in the form of shoulders. These five characteristic absorption features are relatively weak but present in the spectra of $Pb(NO_3)_2$ and $Th(NO_3)_4$, and the long-wavelength absorption features are more easily identified (Figure 2A and Table 1). $LiNO_3$ has sharp and broad absorptions around 1.4 and 1.9 μm (Figure 2A) that are diagnostic of water molecules (Table 2; Hunt, 1977), likely due to the hygroscopic capacity of $LiNO_3$ that leads to the presence of adsorbed water. The 1.81, 2.21 and 2.42 μm features are also discernible in the spectrum of $LiNO_3$, while the 1.94 and 2.06 μm features are merged into the broad ~1.9 μm water absorption band, showing only small shoulders. In Figure 2B, the hydrated salts all have significant water absorption bands around 1.4 and 1.9 μm, but the depth and width of water bands were not observed to relate to the changes in hydration states. $Cu(NO_3)_2•H_2O$, $Fe(NO_3)_3•7H_2O$ and $Zn(NO_3)_2•10H_2O$ have strong absorptions over the 0.35-2.5 μm spectral range likely owing to crystal field effects of their metal ions (Hathaway et al., 1963; Hunt, 1977), while the strong absorptions by $Al(NO_3)_3•9H_2O$ in the 1.0-2.5 μm range are likely attributed to the overtones and combinations of water molecules as well as the Al-OH vibrations. For other hydrated salts in Figure 2B, most of the 1.94, 2.06 and 2.21 μm absorption features of nitrate are strongly influenced by the 1.9 μm water absorption to only show shoulders, while small absorptions or inflections are typically noticeable around 1.81 and 2.42 μm despite some shifts in the absorption feature center positions. The differences in the size or center position of absorption features of different nitrate salts (Figure 2) are likely due to distinct ion pairing effects of different metal ions (Xu et al., 2008). Therefore, the five absorption features at 1.81, 1.94,

242 2.06, 2.21 and 2.42 μm are diagnostic nitrate features, but may overlap with water bands
243 and may also be displaced depending on the cations in the nitrate salts.

244 There are some unique minerals that co-exist with nitrate minerals in the Atacama
245 (Ericksen, 1981) and are likely to co-exist in other similar hyper-arid environments,
246 which may interfere with the nitrate absorptions at some wavelengths. Sulfate minerals
247 such as gypsum ($CaSO_4 \bullet 2H_2O$) and anhydrite ($CaSO_4$) are ubiquitously found in the
248 Atacama, which can be one of the major mineral groups co-existing with nitrate in hyper-
249 arid environments (Ericksen, 1981). The comparison of the spectra of the anhydrous and
250 hydrated forms of two common Atacama sulfate minerals, mirabilite ($Na_2SO_4 \bullet 10H_2O$)
251 and darapskite ($Na_3NO_3SO_4 \bullet H_2O$), indicates that the hydrated forms have stronger
252 absorption features than their anhydrous forms (Figure 3). The reflectance spectrum of
253 anhydrous Na_2SO_4 is nearly flat without absorptions in the VNIR region, suggesting that
254 there are no characteristic absorptions by sulfate group in the VNIR region. No sulfate
255 absorption feature in the VNIR region was also observed in the spectrum of anhydrite
256 ($CaSO_4$) that was archived in the USGS spectral library (Clark et al., 2007). Crowley
257 (1991) measured the VNIR spectrum of thenardite (Na_2SO_4) to find only two broad water
258 bands near 1.4 and 1.9 μm, which, however, were likely accounted for by the presence of
259 fluid inclusions and/or adsorbed water rather than the sulfate group. In addition, the
260 reflectance spectrum of anhydrous darapskite ($Na_3NO_3SO_4$) is nearly identical to that of
261 $NaNO_3$ (Figure 3), also providing a line of evidence of the lack of absorption features for
262 sulfate in the VINR region. The absence of sulfate absorption features in the VNIR
263 region is likely because there are no overtone or combination features of sulfate in the
264 VNIR region owing to the low frequencies of the fundamentals of sulfate in the middle

infrared region (Cloutis et al., 2006). Therefore, the VNIR absorption features in hydrated sulfate minerals are mainly due to the presence of water molecules or possible hydroxyl (OH). The differences between our spectra of mirabilite and anhydrous Na_2SO_4 showed the absorption bands centered at 0.97, 1.21 (with a shoulder), 1.48 (broad, with a shoulder), 1.75, 1.9 (broad) and 2.5 μm (Figure 3), which are accounted for by the overtones and combinations of fundamental vibration modes of the water molecule and the association of S-O bonds and H_2O (~2.4 μm) (Table 2). For sulfate minerals with OH in the crystal structure, the overtones of OH stretching and combinational vibrations of OH stretching and metal-OH bending can also cause absorptions in the VNIR region as indicated in Table 2. These water molecule or OH-related absorptions in hydrated sulfate minerals may overlap with some of the nitrate absorption bands.

Previous studies suggested the major minerals of Atacama regoliths other than nitrate and sulfate minerals are: quartz (SiO_2), anorthite ($CaAl_2Si_2O_8$), albite ($NaAlSi_3O_8$), microcline ($KAlSi_3O_8$), hornblende ($(Ca,Na)_2(Mg,Fe,Al)_5(Al,Si)_8O_{22}(OH)_2$), and chlorine salts (e.g. halite NaCl and sodium perchlorate $NaClO_4$) (Ewing et al., 2006; Wang et al., 2015). Carbonate may also sporadically occur in some parts of the Atacama in the form of calcite ($CaCO_3$). The anhydrous forms of these major interference minerals except carbonate were shown to have no diagnostic absorptions in the VNIR region (Clark et al., 2007; Sutter et al., 2007; Hanley et al. 2015), though some hydrated forms may have absorptions overlapping nitrate features. Carbonate has relatively weak absorptions near 1.88, 2.00, and 2.17 μm overlapping with some nitrate absorption bands, but its most intense absorption occurring near 2.31 μm would not overlap the nitrate absorptions (Clark et al., 1990).

In summary, the characteristic nitrate absorption features around 1.81, 1.94, 2.06, 2.21 and 2.42 μm could mainly be interfered by adsorbed water or hydrated minerals, and therefore, careful inspections should be coupled with the VNIR spectral analysis. However, our measured spectrum of hydrated darapskite shows all of these five absorption bands despite the existence of water of hydration, suggesting the nitrate absorption bands may superimpose on water/metal-OH absorption bands to allow for the identification of nitrate via characteristic absorption features. Though hydrated minerals have been confirmed to exist widely in the hyper-arid settings such as the Atacama or similar planetary environments such as Mars, the interferences of water/metal-OH should depend on the nitrate contents and hydration status of individual samples, and the nitrate absorption features may stand out when high nitrate contents but low hydration degrees are present.

Quantitative relationship between nitrate content and absorption band depth

The anion (chloride, nitrate and sulfate) contents and laboratory spectra of all the regolith samples from the LT, ST and CCP profiles are shown in SI Figures S1 and S2, respectively. The nitrate contents range from 0.4-8.3 wt% in the LT profile, 0-13.7 wt% in the ST profile, and 0.2-36.9 wt% in the CCP profile. Representative spectra are then selected based on spectral diversity and variety of nitrate content and presented in Figure 4. These spectra are relatively flat near 1.81 μm, but have absorption features around 1.9, 2.06 (shoulder), 2.21 and 2.42 μm. As the nitrate content increases, the 1.81, 2.06, 2.42 μm absorptions become more conspicuous and significant, while the 1.9 and 2.21 μm absorptions had relatively small variations in band depths probably because these two absorptions are also accounted for by water/metal-OH (Figure 4). For example, the

311 sample with the second highest nitrate content (19.6 wt%) in the CCP profile starts to
312 have distinct absorptions around 1.81 and 2.06 μm, and the 2.42 μm feature transitions
313 from an inflection to a trough (Figure 4C). Our observations are consistent with the
314 demonstration by Hovis (1966) of prominent 1.81 and 2.42 μm absorption troughs for the
315 sample with 15 wt% $NaNO_3$ compared to no significant absorptions at 1.81 μm and a
316 downward line at 2.42 μm for the sample with 10-12 wt.% $NaNO_3$. However, for the
317 sample with the highest nitrate content (36.9 wt%), the center of the ~1.9 μm band occurs
318 at ~1.94 μm, and the absorption band at ~2.21 μm becomes considerably sharper,
319 probably due to the elevation in the contribution of nitrate relative to water/metal-OH to
320 the absorptions (Figure 4C). These changes are more pronounced in the continuum-
321 removed spectra of the selected CCP samples for the characteristic nitrate absorption
322 features (Figure 5A-D).

323 Correlation analysis indicated a significant positive correlation between nitrate
324 contents and the 2.42 μm absorption band depths in the CCP profile (n=72, Pearson
325 correlation coefficient: 0.53, p=0.000) (Table 3). However, the 2.42 μm absorption band
326 depths remain relatively consistent when nitrate contents range from 0-10 wt% (Figure
327 5F), and significant positive correlations are not observed in the LT and ST profiles that
328 have much lower nitrate contents, suggesting that the 2.42 μm absorption feature is
329 essentially sensitive to high nitrate contents. In addition, the wavelength position of the
330 2.42 μm band minima oscillated between 2.34 and 2.45 μm (Figure 5E). Since the ~2.35
331 μm absorption could be attributed to metal-OH, the samples with the 2.42 μm band
332 minima occurring at ~2.35 μm were excluded for further correlation analysis. Therefore,
333 only the samples with nitrate contents >10 wt% and the band minima occurring at ~2.42

μm were adopted to further investigate the correlation between nitrate contents and the 2.42 μm absorption band depths. The resulted correlation equation shown in Figure 5F should be applicable to quantify the nitrate contents based on the spectral properties of 2.42 μm band. There is also a significant positive correlation between the chloride contents and 2.42 μm band depths in the CCP profile ($p<0.05$, Table 3), likely due to the significant correlation between chloride and nitrate contents (Pearson correlation coefficient: 0.85, $p<0.001$) because of their similar solubilities that lead to similar transport activities and fate in the profile. Instead, no significant positive correlation was found between sulfate contents and the 2.42 μm absorption band depths in any of the three profiles (Table 3). Also, there is a significant negative correlation or no correlation between chloride/nitrate/sulfate contents and the band depths of the 1.81, 1.94 or 2.21 μm absorption features in the three profiles (Table 3), suggesting that other components rather than chloride/nitrate/sulfate mainly account for these features in these Atacama samples.

Therefore, the five nitrate absorption features in the VNIR region can provide general perspectives into the presence or absence of nitrate, and the appearance of 1.81 and 2.06 μm features and the absorption trough around 2.42 μm are typically indicative of large abundances of nitrate. The 2.42 μm can further be used to quantify nitrate contents in samples, especially when nitrate contents are >10 wt%.

Field-based spectral characterization of the Atacama nitrate mine regions

The field spectra have significant atmospheric absorptions around 1.4 and 1.9 μm compared to the laboratory spectra but are consistent with laboratory spectra with most nitrate absorption features prominent (except the 1.81 μm feature mostly disturbed by

357 atmospheric absorptions) (Figure 6). The similarity of Baquedano pit 1 to the LT and ST
358 sites in nitrate contents is evident by their similar spectra with sporadic 1.94 μm
359 absorptions, insignificant 2.06 μm shoulders, identifiable 2.21 μm absorptions and subtle
360 inflections around 2.42 μm (Figures 4A, 4B, 6A and 6C). In contrast, for some samples
361 from the Baquedano, Sierra Gorda and Tama mine sites, there are clearly defined
362 absorption features at 1.94, 2.06 and 2.21 μm, distinct inflections (even troughs) at ~2.42
363 μm, and sporadic absorptions around 1.81 μm in both the laboratory and field reflectance
364 spectra, suggesting relatively high concentrations of nitrate at these three mine tailing
365 sites (Figures 6B and 6D-H). In the Salar de Carmen, there are small but identifiable
366 absorption bands around 1.94 and 2.21 μm, shoulders around 2.06 μm and inflections at
367 ~2.42 μm in some of the field spectra, which together suggested an abundance of nitrate
368 on the surface (Figure 6I). This is consistent with past observations from Whitehead
369 (1920) that proposed the natural efflorescence of sodium nitrate over a large area of the
370 Salar de Carmen. Besides, in view of the yellowish color of the surface, significant
371 absorptions in the ranges of 0.35-0.6 μm and 0.7-1.3 μm (centered at ~0.9 μm) are robust
372 indications of iron (III). The 1.81 and 1.94 μm features in the spectra collected in the
373 Salar de Grande are greatly influenced by atmospheric absorption and difficult to identify
374 (Figure 6J). The 2.06 μm features are almost absent, suggesting relatively low nitrate
375 contents, in line with Stoertz and Ericksen (1974) that the Salar de Grande is dominated
376 by halite minerals. Among these field spectra, one for the Tama mine has a complete set
377 of five absorption features (Figure 6F-black line), indicating the presence of the highest
378 nitrate content. Considering the long wavelength side of the 2.42 μm absorption is subject
379 to significant interferences of instrument noise, its absorption band depth was calculated

to be the differences between the maximum and the minimum on the short wavelength side of the 2.42 μm continuum-removed absorption band (2.25-2.45 μm range). Based on the quantitative relationship demonstrated in Figure 5F, the largest 2.42 μm absorption band depth of 0.33 occurring at the Tama site corresponds to 35.7 wt% nitrate which is consistent with the reported concentration range for the nitrate ores by Ericksen (1981); the samples from the Baquedano, Sierra Gorda and Tama mine and the Salar de Carmen are mostly rich in nitrate with nitrate contents generally >10 wt% (Figure 7). In summary, this work suggests that in situ detection of nitrate is feasible using the field VNIR reflectance spectra by identifying some or all of the five nitrate absorption features, and the 2.42 μm absorption feature could even be used to determine the nitrate contents, showing great potential in implications into nitrate search and quantification on planetary surfaces via remote sensing techniques.

IMPLICATIONS

The recent detection of nitrate, a biochemically accessible form of nitrogen, by the Mars Science Laboratory Curiosity rover adds to the evidence for the habitability of the ancient Martian environment (Stern et al., 2015). Nitrate is naturally added to soils via atmospheric deposition or produced in situ via biological nitrification on Earth. Nitrification, the oxidation of ammonium via nitrifying bacteria, is generally considered to be the dominant mechanism of nitrate accumulation in most soils. Nevertheless, in hyper-arid regions such as the Atacama Desert, the Antarctic McMurdo Dry Valley and the Turpan-Hami basin, stable isotope technique proved that soil nitrate is predominantly from atmospheric deposition in that nitrification is minimized due to the lack of liquid water (Michalski et al., 2003; Qin et al., 2012; Wang et al., 2016). Though the Martian

403 nitrate discovered was also likely produced in the atmosphere rather than biology (Stern
404 et al., 2015), the presence of nitrate suggests the potential evolution of the nitrogen cycle
405 on the Martian surface which could instead provide fixed nitrogen essential for life.
406 Therefore, the discovery of nitrate, together with the evidence of other life-related
407 ingredients like liquid water (Ojha et al., 2015) and organic matter (Freissinet et al.,
408 2015), suggests that Mars might have been more hospital in the ancient past.

409 If any past Martian environments were habitable, they probably existed billions of
410 years ago, when atmospheric nitrogen (as N_2) was estimated to be 3-300mbar, far higher
411 than the present-day Martian atmosphere of ~0.2 mbar (Mancinelli, 1996). If there was
412 abundant nitrogen, where has it gone? Conversion of N_2 into nitrate by fixation and its
413 storage in the Martian regolith is one possibility. Nitrate production in Martian
414 atmosphere has been proposed to be initiated by the formation of nitric oxide (NO) by
415 interaction between atmospheric CO_2/N_2 and a high energy source, such as cosmic rays,
416 ultra-violet (UV) radiation (Yung et al., 1977), lightning, volcanism (Segura and
417 Navarro-González, 2005) or meteor/comet impacts (Manning et al., 2009). Each of these
418 processes could possibly lead to different distribution of nitrate minerals in the Martian
419 regolith. For examples, nitrogen fixation by volcanism might lead to regional deposits,
420 whereas UV radiation would be more evenly distributed. This suggests that the
421 exploration of nitrate mineral distributions could determine which fixation process was
422 most important. In addition, the relationship between nitrate and other soluble salts like
423 chloride, sulfate and perchlorate that are known to widely exist on Mars and hypothesized
424 to have similar origins of atmospheric deposition can provide information for Martian
425 surface conditions and their link to atmospheric photochemical processes, for example

426 the formation mechanisms of individual salts and the post-depositional processing of
427 nitrate (Stern et al., 2017). Hence, mapping the extent and abundance of nitrate as well as
428 identifying the co-existing mineral assemblages is important for understanding the nature
429 of pedogenesis and atmospheric chemistry on Mars.

430 Compared to the SAM instrument suite on Mars Curiosity rover, reflectance
431 spectroscopy offers advantages for investigating the areal extent and abundance of nitrate
432 as well as providing a complete picture of the mineralogical composition of samples in a
433 non-destructive fashion. CRISM (0.36-3.9 μm range, 6.55 nm resolution) aboard the
434 Mars Reconnaissance Orbiter and OMEGA (0.5-5.2 μm range, 7-20 nm resolution)
435 aboard the Mars Express mission are two imaging spectrometers currently orbiting Mars,
436 which cover the VNIR domain and should be capable of detecting the nitrate absorption
437 features. Though these CRISM and OMEGA data played important roles in detecting
438 sulfates and chlorides on Mars (Gendrin et al., 2005; Langevin et al., 2005; Bibring et al.,
439 2006; Murchie et al., 2009; Farrand et al., 2009), nitrate has not been detected by either
440 of these two instruments. Nevertheless, spectra that were previously attributed to
441 hydrated sulfate minerals have absorption features overlapping the characteristic
442 absorption bands of nitrate revealed in this study. For example, the OMEGA reflectance
443 spectra of the northern circumpolar region, and outcrops in Valles Marineris, Margaritifer
444 Terra, and Terra Meridiani of Mars that were reported to indicate the presence of
445 calcium-rich sulfate (Gendrin et al., 2005), kieserite or polyhydrated sulfates (Langevin et
446 al., 2005) all had five characteristic absorption bands of nitrate around 1.81, 1.94, 2.06,
447 2.21 and 2.42 μm, though their 1.81 and 2.06 μm absorptions were usually not discussed.
448 This is intriguing since nitrate likely co-exists with the hydrated sulfate minerals, or there

might be confusion between sulfates and nitrates during the spectral identification on Mars. In addition, the nitrate absorptions also overlap with several oxychlorine salts, especially $Ca(ClO_4)_2 \bullet 4H_2O$, as shown by Hanley et al. (2015). Therefore, additional detailed analysis of subtle differences between nitrate and hydrated sulfate/oxychlorine minerals is needed, and future comparisons and spectral studies of Mars should include the 0.35-2.5 μm nitrate spectra presented here. Future work is needed on the spectral characterization of more complex nitrate minerals, like ungemachite $[K_3Na_8Fe(III)(SO_4)_6(NO_3)_2 \cdot 6(H_2O)]$, buttgenbachite $[Cu_{19}(NO_3)_2Cl_4(OH)_{32} \cdot 2H_2O]$ and humberstonite $[K_3Na_7Mg_2(SO_4)_6(NO_3)_2 \cdot 6H_2O]$. This will further fill gaps in the reference spectral library for possible "exotic" nitrate mineral search on Mars; however, we acknowledge these pure complex nitrate minerals are difficult to obtain.

This study presents a wide range of laboratory and field spectra for nitrate salts and nitrate-abundant regolith samples which will supplement existing spectral libraries and provide suitable criteria for identification of different nitrate minerals using hyperspectral sensors. Progress towards mapping the landscape position of astrobiologically-important nitrate via orbital spectroscopy will have important implications for surface processes, propose future Martian missions where nitrate is a priority and eventually help with the seeking for life on Mars. Considering nitrate and chloride salts have similar solubility and the common co-occurrence of nitrate and chloride minerals at Mars analog sites (Ericksen, 1981; Qin et al., 2012), the nitrate search will first be advised to follow the chloride deposits on Mars. Future Martian nitrate detection will be augmented by several upcoming landed spectrometers, i.e. MicrOMEGA (0.9-3.5 μm range, 20 nm resolution) (Leroi et al., 2009) and MA_MISS (0.8-2.8 μm range, 20 nm resolution) (Coradini et al.,

472 2001) which will both be equipped with the ESA 2018 ExoMars rover, as well as the
473 SuperCam (0.4-0.9 μm range, <1 nm resolution and 1.3-2.6 μm range, 0.02 μm resolution)
474 that will fly on the 2020 Mars rover (Wiens et al., 2017), and their synergies with the
475 complementary microscopy and chemical analysis techniques.

476 **ACKNOWLEDGMENTS**

477 The data collection was partially supported by the United States National Science
478 Foundation Grant (EAR 0922114) to GM, the Mineralogical Society of America
479 Graduate Student Research Grant to FW, and several fellowships from Purdue University
480 to FW (Purdue Climate Change Research Center fellowship, Purdue Research
481 Foundation research assistantship and Purdue Bilsland Dissertation fellowship). The data
482 analysis and paper writing were mainly conducted at Peking University Shenzhen
483 Graduate School supported by the postdoctoral funding from Peking University Shenzhen
484 Graduate School. We thank Raul Ochoa for his assistance in the lab and field. We are
485 also grateful to Keith Putirka (editor), Javier Cuadros (editor) and two reviewers for
486 valuable suggestions that helped greatly improve this paper.

487 **REFERENCES CITED**

488 Angelis, S.D., Sanctis, M.C.D., Ammannito, E., Carli, C., Iorio, T. D., & Altieri, F.
489 (2014). The ma_miss instrument performance, i: analysis of rocks powders by martian
490 vnir spectrometer. Planetary & Space Science, 101(2), 89-107.
491 Banin, A., Han, F.X., Kan, I., and Cicelsky, A. (1997) Acidic volatiles and the Mars soil.
492 Journal of Geophysical Research-Planets, 102, 13341-13356.

493 Bao, H.M., and Gu, B.H. (2004) Natural perchlorate has a unique oxygen isotope
494 signature. Environmental Science and Technology, 38, 5073-5077.
495 Bao, H., Jenkins, K.A., Khachaturyan, M., and Dıáz, G.C. (2004) Different sulfate
496 sources and their post-depositional migration in Atacama soils. Earth and Planetary
497 Science Letters, 224, 577-587.
498 Bibring, J.P., and Team, T.O. (2006) Global mineralogical and aqueous Mars history
499 derived from OMEGA/Mars Express data. Science, 312, 400-404.
500 Boonmung, S., and Riley, M.R. (2003) Quantitative analysis of added ammonium and
501 nitrate in silica sand and soil using diffuse reflectance infrared spectroscopy.
502 Spectroscopy Letters, 36, 251-274.
503 Clark, R.N., King, T.V.V., Klejwa, M., Swayze, G.A., and Vergo, N. (1990) High
504 spectral resolution reflectance spectroscopy of minerals. Journal of Geophysical
505 Research Solid Earth, 95(B8), 12653-12680.
506 Clark, R.N., Swayze, G.A., Wise, R., Livo, E., Hoefen, T., Kokaly, R., and Sutley, S.J.
507 (2007) USGS digital spectral library splib06a: U.S. Geological Survey, Digital Data
508 Series 231 (Online). Available: http://speclab.cr.usgs.gov/spectral.lib06 (accessed
509 October 15, 2016). U.S. Geological Survey, Denver, Colorado.
510 Cloutis, E.A., Hawthorne, F.C., Mertzman, S.A., Krenn, K., Craig, M.A., Marcino, D.,
511 Methot, M., Strong, J., Mustard, J.F., Blaney, D.L., Bell, J.F., Vilas, F. (2006)
512 Detection and discrimination of sulfate minerals using reflectance spectroscopy.
513 Icarus, 184, 121-157.

514 Cloutis, E., Berg, B., Mann, P., and Applin, D. (2016) Reflectance spectroscopy of low
515 atomic weight and Na-rich minerals: borates, hydroxides, nitrates, nitrites, and
516 peroxides. Icarus, 264, 20-36.
517 Coradini, A., Piccinoni, G., Amici, S., Bianchi, R., Capaccioni, F., Capria, M.T., De
518 Sanctis, M.C., Di Lellis, A.M., Espinasse S., Federico, C., Fonti, S., Arnold, G.,
519 Atreya, S.K., Owen, T., Blecka, M., Bini, A., Cosi, M., Pieri, S., Tacconi, M. (2001)
520 MA_MISS: Mars multispectral imager for subsurface studies. Advances in Space
521 Research, 28, 1203-1208.
522 Crowley, J.K. (1991) Visible and near-infrared (0.4-2.5 μm) reflectance spectra of playa
523 evaporite minerals. Journal of Geophysical Research Solid Earth, 96, 16231-16240.
524 Ehsani, M.R., Upadhyaya, S.K., Fawcett, W.R., Protsailo, L.V., and Slaughter D. (2001)
525 Feasibility of detecting soil nitrate content using a mid-infrared technique.
526 Transactions of the Asae, 44, 1931-1940.
527 Ericksen, G.E. (1981) Geology and origin of the Chilean nitrate deposits. U.S. Geological
528 Survey Professional Paper 1188, 37 p.
529 Ericksen, G.E., and Mrose, M.E. (1970) Mineralogical studies of the nitrate deposits of
530 Chile: VII Darapskite, $Na_3(NO_3)(SO_4)\bullet H_2O$. The American Mineralogist, 55, 1500-
531 1517.
532 Ewing, S., Sutter, B., Owen, J., Nishiizumi, K., Sharp, W., Cliff, S., Perry, K., Dietrich,
533 W., McKay, C., and Amundson, R. (2006) A threshold in soil formation at Earth's
534 arid-hyperarid transition. Geochimica et Cosmochimica Acta, 70, 5293–5322.

535 Farrand, W.H., Glotch, T.D., Rice, J.W.Jr., Hurowitz, J.A., and Swayze, G.A. (2009)
536 Discovery of jarosite within the Mawrth Vallis region of Mars: implications for the
537 geologic history of the region. Icarus, 204(2), 478-488.
538 Freissinet, C., Glavin, D.P., Mahaffy, P.R., Miller, K.E., Eigenbrode, J.L., Summons,
539 R.E., Brunner, A.E., Buch, A., Szopa, C., Archer Jr., P.D., Franz, H.B., Atreya, S.K.,
540 Brinckerhoff, W.B., Cabane, M., Coll, P., Conrad, P.G., Des Marais, D.J., Dworkin,
541 J.P., Fairén, A.G., François, P., Grotzinger, J.P., Kashyap, S., ten Kate, I.L., Leshin,
542 L.A., Malespin, C.A., Martin, M.G., Martin-Torres, F.J., McAdam, A.C., Ming, D.W.,
543 Navarro-González, R., Pavlov, A.A., Prats, B.D., Squyres, S.W., Steele, A., Stern,
544 J.C., Sumner, D.Y., Sutter, B., Zorzano, M.-P. and the MSL Science Team (2015),
545 Organic molecules in the Sheepbed Mudstone, Gale Crater, Mars. Journal of
546 Geophysical Research-Planets, 120, 495-514.
547 Gendrin, A., Mangold, N., Bibring, J.P., Langevin, Y., Gondet, B., Poulet, F., Bonello, G.,
548 Quantin, C., Mustard, J., Arvidson, R., and LeMouélic, S. (2005) Sulfates in Martian
549 layered terrains: the OMEGA/Mars Express view. Science, 307, 1587-91.
550 Hanley, J., Dalton, J.B., Chevrier, V.F., Jamieson, C.S., and Barrows, R.S. (2015)
551 Reflectance spectra of hydrated chlorine salts: the effect of temperature with
552 implications for Europa. Journal of Geophysical Research Planets, 119, 2370-2377.
553 Hathaway, B.J., Holah, D.G., and Hudson, M. (1963) The infrared and reflectance spectra
554 of some transition-metal nitrate and perchlorate dihydrates. Journal of the Chemical
555 Society, 4586-4589.
556 Hecht, M.H., Kounaves, S.P., Quinn, R.C., West, S.J., Young, S.M.M., Ming, D.W.,
557 Catling, D.C., Clark, B.C., Boynton, W.V., Hoffman, J. L., DeFlores, P.,

558 Gospodinova, K., Kapit, J., and Smith, P.H. (2009) Detection of perchlorate and the
559 soluble chemistry of Martian soil at the Phoenix lander site. Science, 325, 64-67.
560 Houston, J. (2006) Variability of precipitation in the Atacama Desert: Its causes and
561 hydrological impact. International Journal of Climatology, 26, 2181-2198.
562 Houston, J., and Hartley, A.J. (2003) The central Andean west slope rainshadow and its
563 potential contribution to the origin of hyper-aridity in the Atacama Desert.
564 International Journal of Climatology, 23, 1453-1464.
565 Hovis, W.A. (1966) Infrared spectral reflectance of some common minerals. Applied
566 Optics, 5, 245-248.
567 Hunt, G.R. (1977) Spectral signatures of particulate minerals in the visible and near
568 infrared. Geophysics, 42, 501-513.
569 Jahn, B.R., Linker, R., Upadhyaya, S.K., Shaviv, A., Slaughter, D.C., and Shmulevich, I.
570 (2006) Mid-infrared spectroscopic determination of soil nitrate content. Biosystems
571 Engineering, 94, 505-515.
572 Kokaly, R.F., and Clark, R.N. (1999) Spectroscopic determination of leaf biochemistry
573 using band-depth analysis of absorption features and stepwise multiple linear
574 regression. Remote Sensing of Environment, 67, 267-287.
575 Langevin, Y., Poulet, F., Bibring, J. P., and Gondet, B. (2005) Sulfates in the north polar
576 region of mars detected by OMEGA/Mars Express. Science, 307(5715), 1584-6.
577 Leroi, V., Bibring, J.P., and Berthe, M. (2009) Micromega/IR: Design and status of a
578 near-infrared spectral microscope for in situ analysis of Mars samples. Planetary and
579 Space Science, 57, 1068-1075.

580 Mancinelli, R.L. (1996) The search for nitrogen compounds on the surface of Mars.
581 Pergamon Press Ltd, Oxford.
582 Manning, C. V., K. J. Zahnle and C. P. McKay, Impact processing of nitrogen on early
583 Mars, *Icarus, 199*(2), 273-285, 2009.
584 Michalski, G., Böhlke, J.K., and Thiemens, M. (2004) Long term atmospheric deposition
585 as the source of nitrate and other salts in the Atacama Desert, Chile: New evidence
586 from mass-independent oxygen isotopic compositions. Geochimica et Cosmochimica
587 Acta, 68, 4023-4038.
588 Moorcroft, M.J., Davis, J., and Compton, R.G. (2001) Detection and determination of
589 nitrate and nitrite: a review. Talanta 54, 785-803.
590 Murchie, S.L., Mustard, J.F., Ehlmann, B.L., Milliken, R.E., Bishop, J.L., Mckeown,
591 N.K., et al. (2009) A synthesis of martian aqueous mineralogy after 1 mars year of
592 observations from the mars reconnaissance orbiter. Journal of Geophysical Research
593 Planets, 114(E2), 0-6.
594 Nair, H., Allen, M., Anbar, A.D., Yung, Y.L., and Clancy, R.T. (1994) A photochemical
595 model of the Martian atmosphere. Icarus, 111, 124-150.
596 Navarro-González, R., Rainey, F., Molina, P., Bagaley, D., Hollen, B., de la Rosa, J.,
597 Small, A., Quinn, R., Grunthaner, F., and Caceres, L. (2003) Mars-like soils in the
598 Atacama Desert, Chile, and the dry limit of microbial life. Science, 302, 1018-1021.
599 Ojha, L., Wilhelm, M.B., Murchie, S.L., McEwen, A.S., Wray, J.J., Hanley, J., Massé, M.
600 and Chojnacki, M. (2015) Spectral evidence for hydrated salts in recurring slope
601 lineae on Mars. Nature Geoscience, 8, 829-832.

602 Osterloo, M.M., Hamilton, V.E., Bandfield, J.L., Glotch, T.D., Baldridge, A.M.,
603 Christensen, P.R., Tornabene, L.L., and Anderson, F.S. (2008) Chloride-bearing
604 materials in the southern highlands of Mars. Science, 319, 1651-1654.
605 Qin, Y., Li, Y., Bao, H., Liu, F., Hou, K., Wan, D. and Zhang, C. (2012) Massive
606 atmospheric nitrate accumulation in a continental interior desert, northwestern China.
607 Geology, 40, 623-626.
608 Segura, A. and Navarro-González, R. (2005) Nitrogen fixation on early Mars by volcanic
609 lightning and other sources. Geophysical Research Letter, 32, 215-236.
610 Seinfeld, J.H. and Pandis, S.N. (2006) Atmospheric Chemistry and Physics: From air
611 Pollution to Climate Change. John Wiley & Sons, New York.
612 Sinfield, J.V., Fagerman, D., and Colic O. (2010) Evaluation of sensing technologies for
613 on-the-go detection of macro-nutrients in cultivated soils. Computers and Electronics
614 in Agriculture, 70, 1-18.
615 Squyres, S.W., Grotzinger, J.P., Arvidson, R.E., Bell, J.F., Calvin, W., Christensen, P.R.,
616 Clark, B.C., Crisp, J.A., Farrand, W.H., Herkenhoff, K.E., Johnson, J.R., Klingelhofer,
617 G., Knoll, A. H., McLennan, S.M., McSween, H.Y., Morris, R.V., Rice, J.W., Rieder,
618 R. and Soderblom, L.A. (2004) *In situ* evidence for an ancient aqueous environment
619 at Meridiani Planum, Mars. Science, 306, 1709-1714.
620 Stern, J.C., Sutter, B., Freissinet, C., Navarro-González, R., McKay, C.P., Douglas, P.A.,
621 Buch, A., Brunner, A.E., Coll, P., Eigenbrode J.L., and others (2015) Evidence for
622 indigenous nitrogen in sedimentary and aeolian deposits from the Curiosity rover
623 investigations at Gale crater, Mars. Proceedings of the National Academy of Sciences,
624 112, 4245-4250.

625 Stern, J.C., Sutter, B., Jackson, W.A., Navarro-González, R., Mckay, C.P., Ming, D.W.,
626 Archer, P.D. and Mahaffy, P.R. (2017). The nitrate/(per)chlorate relationship on Mars.
627 Geophysical Research Letters, 44, 2643-2651.
628 Stoertz, G.E., and Ericksen, G.E. (1974) Geology of salars in northern Chile. U.S.
629 Geological Survey Professional Paper, 811, 65p.
630 Sutter, B., Dalton, J. Ewing S.A., Amundson R., and McKay C.P. (2007) Terrestrial
631 analogs for interpretation of infrared spectra from the Martian surface and subsurface:
632 sulfate, nitrate, carbonate, and phyllosilicate-bearing Atacama Desert soils. Journal of
633 Geophysical Research, 112, G04S10.
634 Wang, F., Ge, W.S., Luo, H., Seo, J.H., and Michalski, G. (2016) Oxygen-17 anomaly in
635 soil nitrate: A new precipitation proxy for desert landscapes. Earth and Planetary
636 Science Letters, 438: 103-111.
637 Wang, F., Michalski, G., Seo, J.H., Granger, D.E., Lifton, N., and Caffee M. (2015)
638 Beryllium-10 concentrations in the hyper-arid soils in the Atacama Desert, Chile:
639 Implications for arid soil formation rates and El Niño driven changes in Pliocene
640 precipitation. Geochimica et Cosmochimica Acta, 160, 227-242.
641 Watters, W.A., Grotzinger, J.P., Bell, J., Grant, J., Hayes A.G., Li, R.X., Squyres, S.W.,
642 Zuber, M.T. (2011) Origin of the structure and planform of small impact craters in
643 fractured targets: Endurance Crater at Meridiani Planum, Mars. Icarus, 211, 472-497.
644 Whitehead, W.L. (1920) The Chilean nitrate deposits. Economic Geology, 15, 187-224.
645 Wiens, R.C., Maurice, S., and Perez, F.R. (2017). The SuperCam remote sensing
646 instrument suite for the mars 2020 rover: A preview. Spectroscopy (Santa Monica),
647 32, 50-55.

Xu, M., Larentzos, J.P., Roshdy, M., Criscenti, L.J., and Allen, H.C. (2008) Aqueous divalent metal-nitrate interactions: hydration versus ion pairing. Physical Chemistry Chemical Physics, 10, 4793-4801.

Yung, Y.L., Strobel, D.F., Kong, T.Y., and McElroy, M.B. (1977) Photochemistry of Nitrogen in Martian Atmosphere. Icarus, 30, 26-41.

Yung, Y. L. and W. B. DeMore, Photochemistry of Planetary Atmospheres, 1998.

This is a preprint, the final version is subject to change, of the American Mineralogist (MSA)
Cite as Authors (Year) Title. American Mineralogist, in press.
DOI: http://dx.doi.org/10.2138/am-2018-6141

655 **Table 1**

656 **Positions of the 1.5-2.5 µm absorption band minima for metal nitrate salts**

657 **(uncertainties ≤10 nm)**

Nitrate salts	Minima of absorption bands, µm
Anhydrous nitrate	
KNO_3	1.83, 1.95 (shoulder), 1.97, 2.06 (shoulder), 2.10, 2.20 (shoulder), 2.25, 2.42 (shoulder), 2.47
$NaNO_3$	1.80, 1.92 (shoulder), 1.94, 2.04 (shoulder), 2.06, 2.18 (shoulder), 2.22, 2.43, 2.47 (shoulder)
$Pb(NO_3)_2$	1.83, 1.98, 2.10, 2.26, 2.43 (shoulder), 2.47
$Th(NO_3)_4$	1.80 (shoulder), 1.86, 1.95, 2.01, 2.06, 2.12, 2.17, 2.25 (shoulder), 2.29, 2.33 (shoulder), 2.45
$LiNO_3$	1.75, 1.81, 1.98, 2.04 (shoulder), 2.17, 2.45
Hydrated nitrate	
$Cu(NO_3)_2•H_2O$	1.69 (shoulder), 1.80, 1.95, 2.00, 2.18 (shoulder), 2.38 (shoulder), 2.50
$Cd(NO_3)_2•4H_2O$	1.74, 1.80, 1.94, 1.98 (shoulder), 2.08, 2.17 (shoulder), 2.42, 2.50
$Zr(NO_3)_4•5H_2O$	1.79 (shoulder), 1.92, 2.28 (shoulder), 2.50
$Co(NO_3)_2•6H_2O$	1.72, 1.80, 1.95, 2.22, 2.38
$La(NO_3)_3•6H_2O$	1.78, 1.94, 2.19, 2.47 (broad)
$Mg(NO_3)_2•6H_2O$	1.55 (shoulder), 1.74 (shoulder), 1.78, 1.95, 2.15 (shoulder), 2.24 (shoulder), 2.40 (shoulder), 2.50
$Ni(NO_3)_2•6H_2O$	1.62 (shoulder), 1.83, 1.95, 2.06 (shoulder), 2.41, 2.50
$UO_2(NO_3)_2•6H_2O$	1.74, 1.93 (shoulder), 1.99, 2.19 (shoulder), 2.42 (shoulder), 2.50
$Fe(NO_3)_3•7H_2O$	1.79 (shoulder), 1.94, 2.50
$Al(NO_3)_3•9H_2O$	1.76 (shoulder), 1.94, 2.05 (shoulder), 2.37 (shoulder), 2.498
$Zn(NO_3)_2•10H_2O$	1.72 (shoulder), 1.82 (shoulder), 1.95, 2.21 (shoulder), 2.36 (shoulder), 2.50

658

659 **Table 2**

660 **Modes and positions of 0.35-2.5 μm absorption features relevant to this study**

661 **(summarized from previous studies)**

Mode	μm
Water molecule (Hunt, 1977)	
$2\upsilon_1+\upsilon_3$	0.942
$\upsilon_1+\upsilon_2+\upsilon_3$	1.135
$\upsilon_1+\upsilon_3$	1.38
$2\upsilon_1+\upsilon_3$	1.454
$\upsilon_2+\upsilon_3$	1.875
Hydroxyl (Hunt, 1977; Clark et al., 1990)	
$3\upsilon_{OH}$	0.95
$2\upsilon_{OH}$	1.4
Al-OH	2.2
Mg-OH	2.3
Fe-OH	2.29
Nitrate (Sutter et al., 2007; Cloutis et al., 2016)	
$4\upsilon_3$	1.81
$3\upsilon_3+\upsilon_2+\upsilon_L$	1.94
$3\upsilon_3+\upsilon_4$	2.06
$2\upsilon_3+2\upsilon_2$	2.21
$3\upsilon_3$	2.42
Sulfate (Gendrin et al., 2005)	
Association of S-O bonds and H_2O	2.4
Carbonate (Clark et al., 1990)	
$\upsilon_1+3\upsilon_3$	1.88
$2\upsilon_1+2\upsilon_3$	2.00
$\upsilon_1+2\upsilon_3+\upsilon_4$ or $3\upsilon_1+2\upsilon_4$	2.17
$3\upsilon_3$	2.31

662

This is a preprint, the final version is subject to change, of the American Mineralogist (MSA)
Cite as Authors (Year) Title. American Mineralogist, in press.
DOI: http://dx.doi.org/10.2138/am-2018-6141

663 **Table 3**

664 **Coefficients of Pearson correlation between anion contents and continuum-removed**

665 **band depths of nitrate absorption features for the Atacama regolith samples**

Contents	Continuum-removed band depths			
	1.81 μm	**1.94 μm**	**2.21 μm**	**2.42 μm**
LT profile				
Chloride	-0.04	**-0.60****	**-0.42****	0.10
Nitrate	-0.03	**-0.52****	**-0.40****	0.20
Sulfate	0.03	-0.28	**-0.43****	0.15
ST profile				
Chloride	-0.18	-0.15	**-0.46****	-0.09
Nitrate	-0.20	-0.16	**-0.43****	-0.14
Sulfate	**-0.38****	**-0.31***	**-0.60****	**-0.34***
CCP profile				
Chloride	**-0.32****	**-0.33****	-0.16	**0.30***
Nitrate	**-0.28***	**-0.27***	-0.07	**0.53****
Sulfate	0.23	0.09	-0.08	-0.12

666 The values in bold indicate the existence of significant correlations between absorption
667 band depths and anion contents. *indicates the significant level <0.05, while **indicates
668 the significant level <0.01.

669

This is a preprint, the final version is subject to change, of the American Mineralogist (MSA)
Cite as Authors (Year) Title. American Mineralogist, in press.
DOI: http://dx.doi.org/10.2138/am-2018-6141

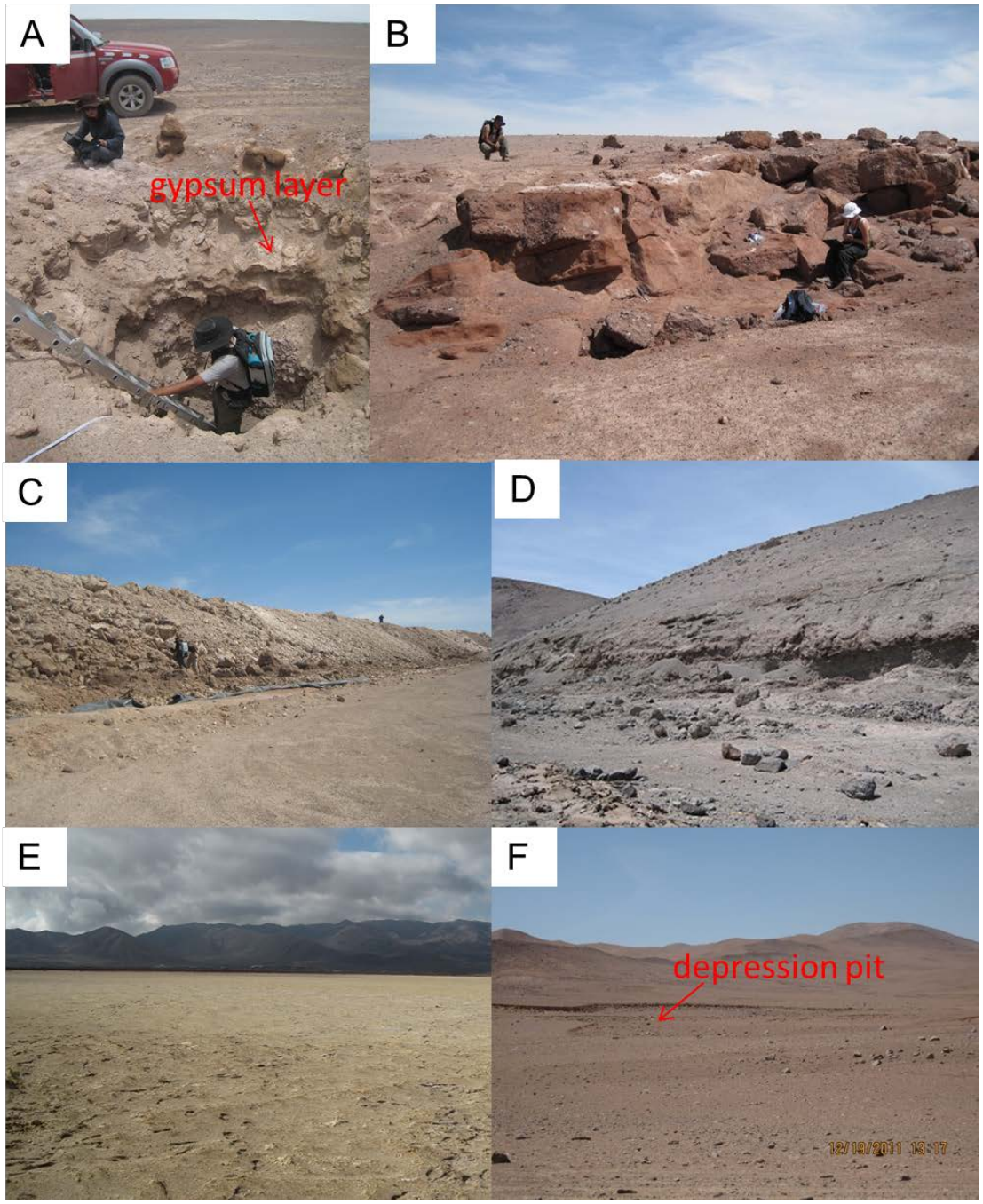

Figure 1

Field pictures of Baquedano pit 1 (A), Baquedano mine (B), Sierra Gorda mine (C), Tama mine (D), Salar de Carmen (E) and Salar de Grande (F) sites where the field reflectance spectra were collected.

This is a preprint, the final version is subject to change, of the American Mineralogist (MSA)
Cite as Authors (Year) Title. American Mineralogist, in press.
DOI: http://dx.doi.org/10.2138/am-2018-6141

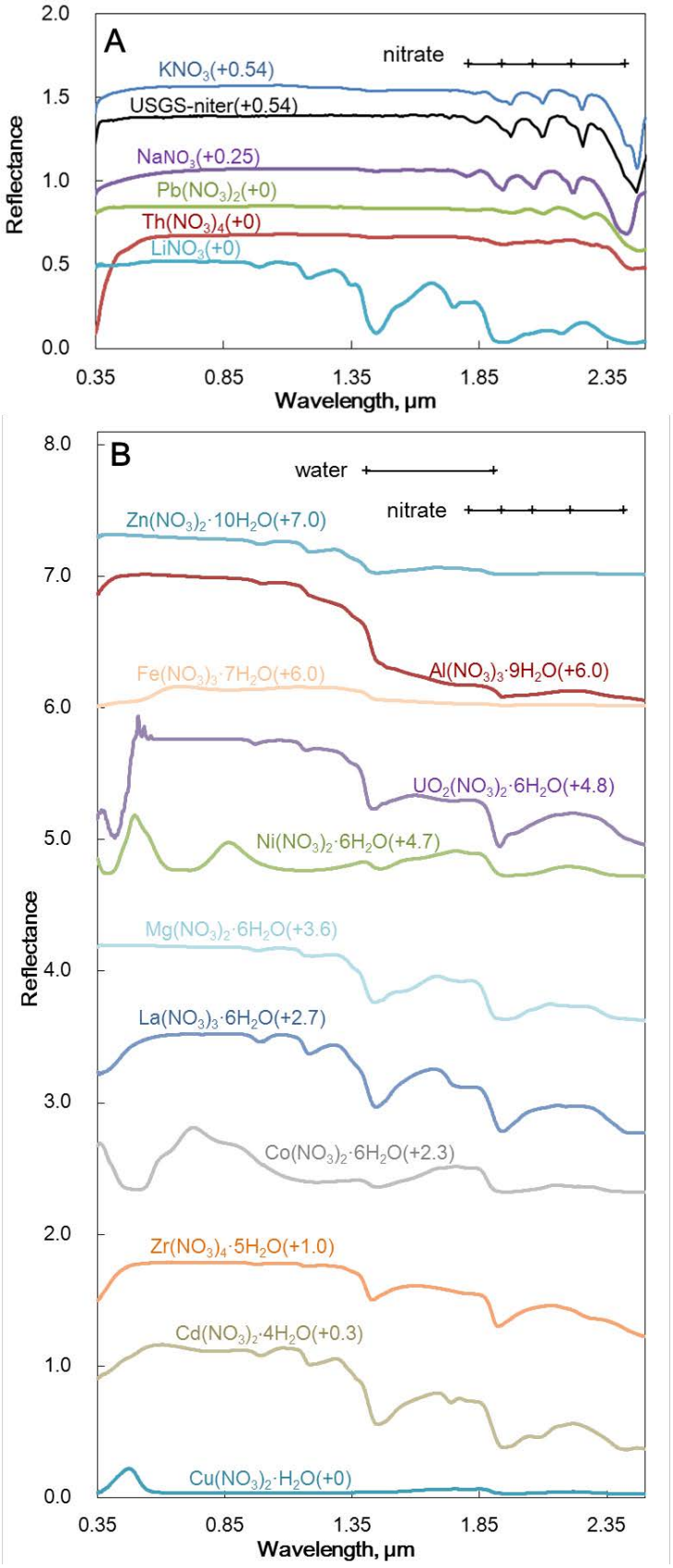

675

676 **Figure 2**

677 **Laboratory reflectance spectra of metal nitrate salts without water of hydration (A;**
678 **except $LiNO_3$, see text) and with water of hydration (B). The USGS-niter spectrum**
679 **is for the mineral niter (KNO_3) from the USGS spectral library archived by Clark et**
680 **al. (2007). The positions of nitrate and molecular water absorptions are indicated by**
681 **the bars on the top of the charts. For clarity, the spectra are offset by an additive**
682 **factor listed in the parentheses after the mineral names or chemical formulae in the**
683 **charts.**

This is a preprint, the final version is subject to change, of the American Mineralogist (MSA)
Cite as Authors (Year) Title. American Mineralogist, in press.
DOI: http://dx.doi.org/10.2138/am-2018-6141

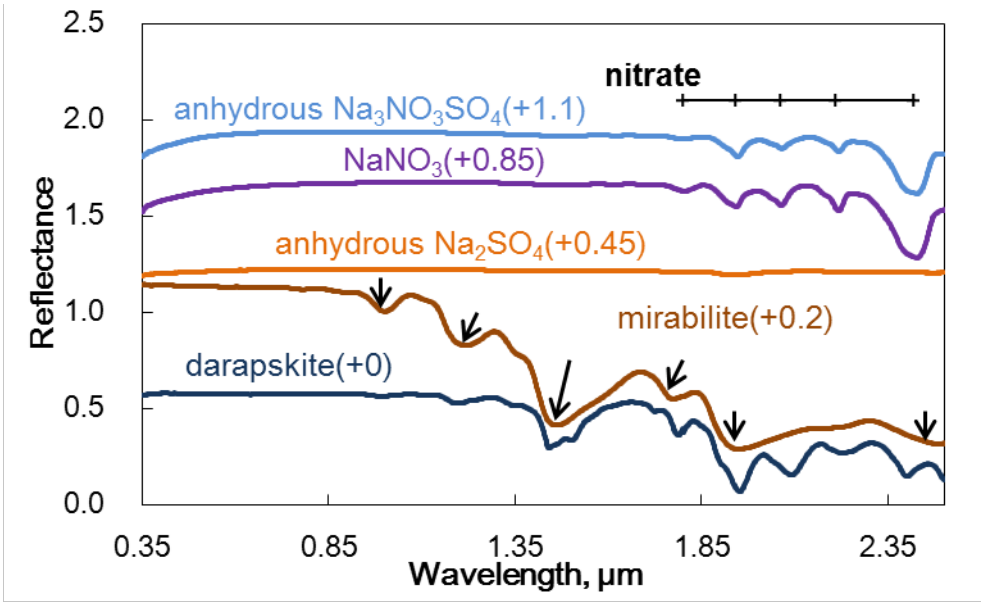

Figure 3

Comparison of laboratory reflectance spectra of the anhydrous and hydrated forms of two common Atacama sulfate minerals (i.e. mirabilite Na_2SO_4•$10H_2O$ and darapskite $Na_3NO_3SO_4$•H_2O). The arrows delineate the water/hydroxyl-related absorption features. The positions of nitrate absorption features as shown in Table 2 are indicated by the bars on the top of the chart. For clarity, the spectra are offset by a factor (positive: additive) listed in the parentheses after the mineral names or chemical formulae in the chart.

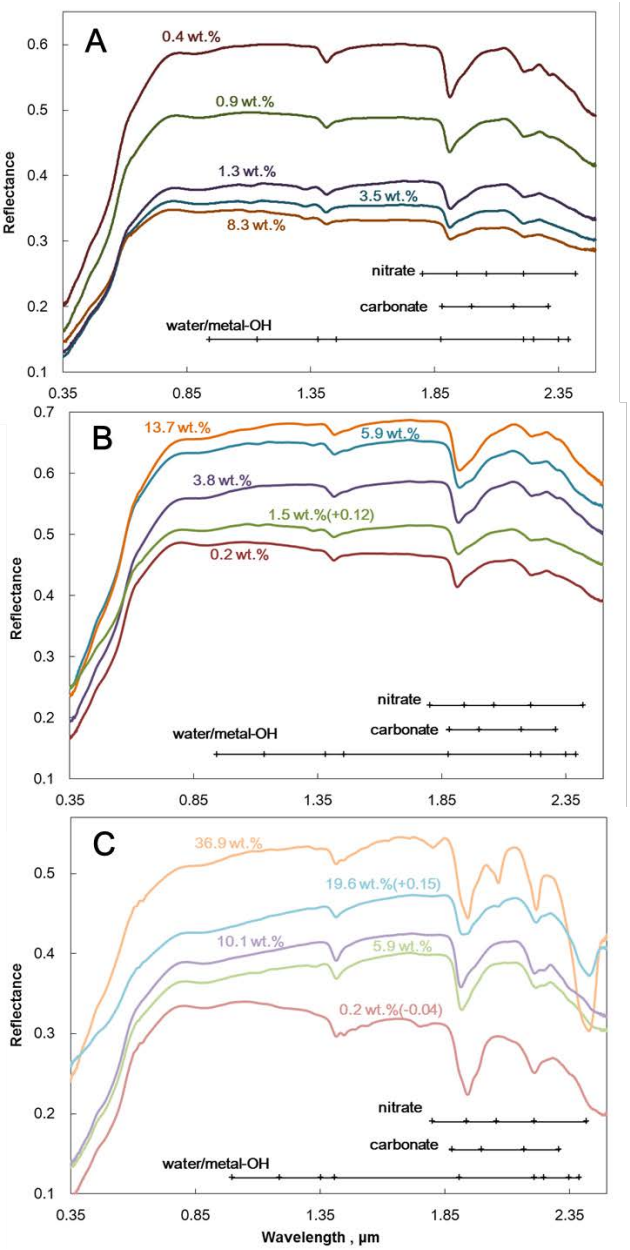

Figure 4

Representative laboratory reflectance spectra of regolith samples from the LT (A), ST (B) and CCP (C) profiles. The positions of absorption features of nitrate, carbonate and water/metal-OH as shown in Table 2 are indicated by bars in the bottom of the charts. The numbers in the unit of wt% delineate the nitrate contents in the regolith samples. The spectra are arranged according to nitrate contents with

some spectra offset by a factor (positive: additive, negative: minus) listed in the parentheses in the chart.

This is a preprint, the final version is subject to change, of the American Mineralogist (MSA)
Cite as Authors (Year) Title. American Mineralogist, in press.
DOI: http://dx.doi.org/10.2138/am-2018-6141

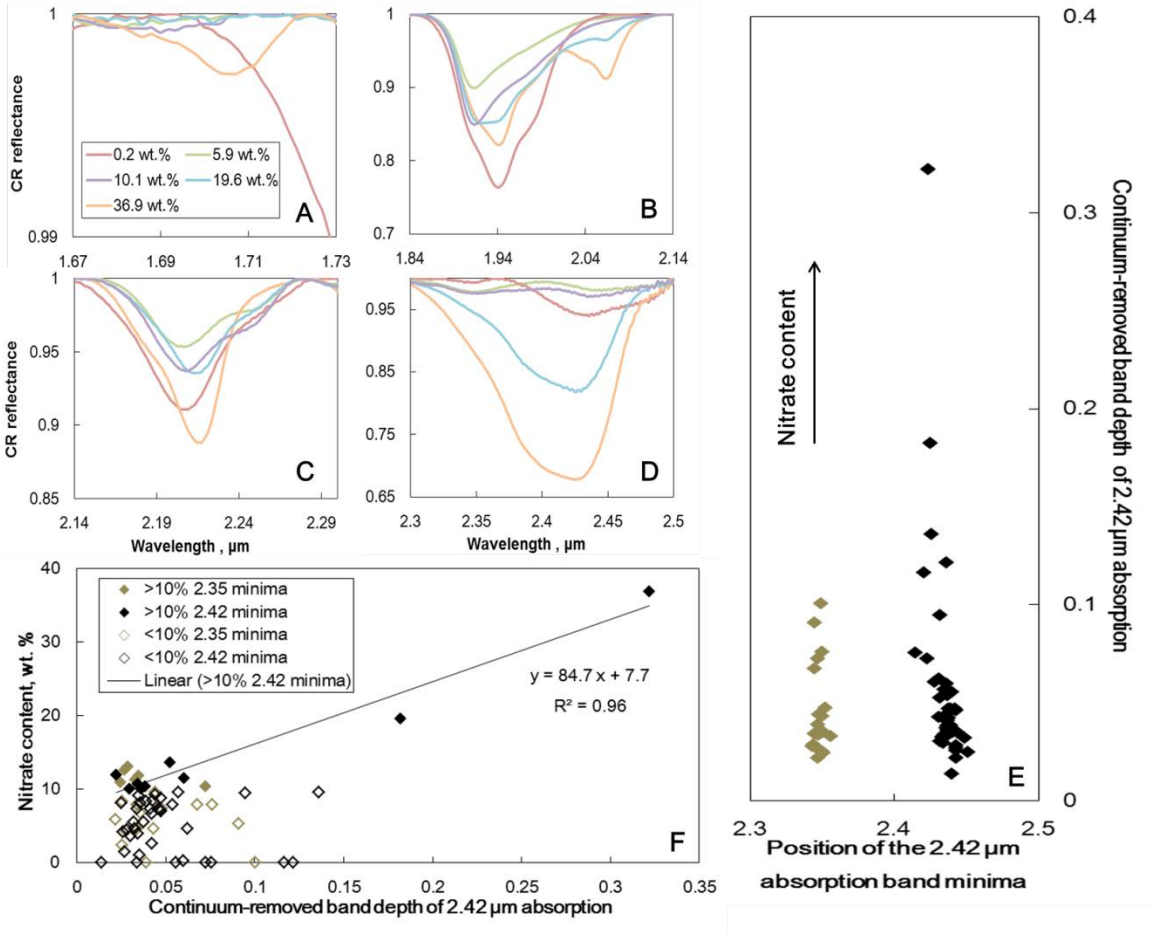

Figure 5

A-D: Continuum-removed (CR) laboratory reflectance spectra of the selected CCP samples (the same as shown in Figure 4C) in different spectral regions with isolated absorption features. E: Points showing the exact wavelengths of the 2.42 µm absorption band minima, between 2.34 and 2.45 µm, versus the band depth. F: Continuum-removed band depths of 2.42 µm feature versus nitrate contents in the CCP profile, with the solid line delineating the fitting line for the samples of nitrate contents >10 wt% and the band minima occurring at ~2.42 µm. The uncertainty in the position of the 2.42 µm absorption band minima is ≤10 nm.

This is a preprint, the final version is subject to change, of the American Mineralogist (MSA)
Cite as Authors (Year) Title. American Mineralogist, in press.
DOI: http://dx.doi.org/10.2138/am-2018-6141

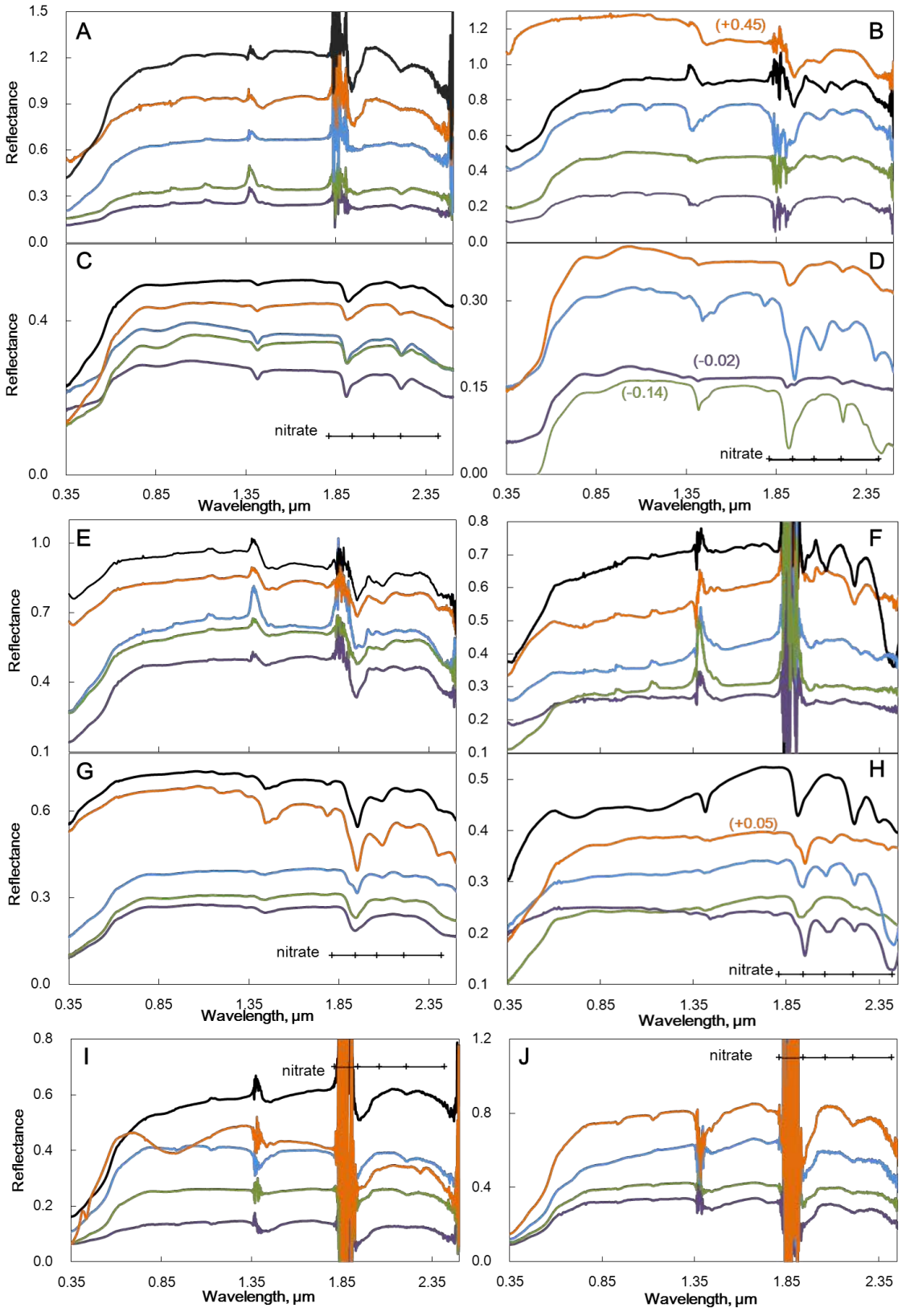

713

Figure 6

Representative reflectance spectra collected in the field (A-Baquedano pit 1, B-Baquedano mine, E-Sierra Gorda mine, F-Tama mine, I-Salar de Carmen, J-Salar de Grande) and in the laboratory for returned samples (C-Baquedano pit 1, D-Baquedano mine, G-Sierra Gorda mine, H-Tama mine). The significant absorptions around 1.4 and 1.9 µm in the field spectra are caused by atmospheric water. The positions of nitrate absorptions are indicated by the bars in the charts. The spectra are arranged for clarity with some spectra offset by a factor (positive: additive, negative: minus) listed in the parentheses in the charts.

This is a preprint, the final version is subject to change, of the American Mineralogist (MSA)
Cite as Authors (Year) Title. American Mineralogist, in press.
DOI: http://dx.doi.org/10.2138/am-2018-6141

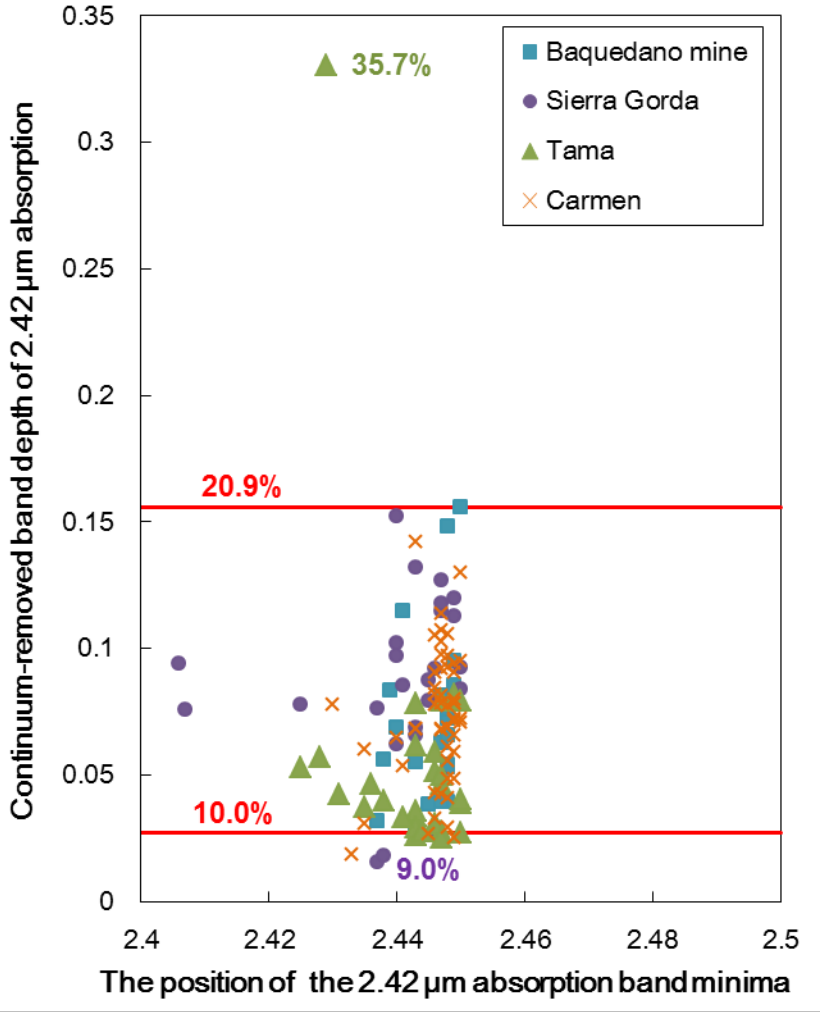

723

724 **Figure 7**

725 **Points showing the exact wavelengths of the band minima versus the continuum-**
726 **removed band depths of the 2.42 µm absorption for the field spectra collected in the**
727 **Atacama nitrate mine regions. The numbers in the chart delineate the nitrate**
728 **contents corresponding to the absorption band depths of the red lines or points**
729 **based on the quantitative relationship shown in Figure 5F. The uncertainty in the**
730 **position of the 2.42 µm absorption band minima is ≤10 nm.**